Chemical interaction of B_4C, B, and C with Mo/Si layered structures

V. I. T. A. de Rooij-Lohmann,[1,a)] L. W. Veldhuizen,[1] E. Zoethout,[1] A. E. Yakshin,[1] R. W. E. van de Kruijs,[1] B. J. Thijsse,[2] M. Gorgoi,[3] F. Schäfers,[3] and F. Bijkerk[1,4]
[1]*FOM Institute for Plasma Physics Rijnhuizen, P.O. Box 1207, 3430 BE Nieuwegein, The Netherlands*
[2]*Department of Materials Science and Engineering, Delft University of Technology, Mekelweg 2, 2628 CD Delft, The Netherlands*
[3]*Helmholtz-Zentrum Berlin für Materialien und Energie GmbH, BESSY II, Albert-Einstein Straße 15, 12489 Berlin, Germany*
[4]*MESA+Institute for Nanotechnology, University of Twente, P.O. Box 217, 7500 AE Enschede, The Netherlands*

(Received 11 August 2010; accepted 15 September 2010; published online 4 November 2010)

To enhance the thermal stability, B_4C diffusion barrier layers are often added to Mo/Si multilayer structures for extreme ultraviolet optics. Knowledge about the chemical interaction between B_4C and Mo or Si, however is largely lacking. Therefore, the chemical processes during annealing up to 600 °C of a Mo/B_4C/Si layered structure have been investigated *in situ* with hard x-ray photoelectron spectroscopy and *ex situ* with depth profiling x-ray photoelectron spectroscopy. Mo/B/Si and Mo/C/Si structures have also been analyzed as reference systems. The chemical processes in these systems have been identified, with two stages being distinguished. In the first stage, B and C diffuse and react predominantly with Mo. $MoSi_x$ forms in the second stage. If the diffusion barrier consists of C or B_4C, a compound forms that is stable up to the maximum probed temperature and annealing time. We suggest that the diffusion barrier function of B_4C interlayers as reported in literature can be caused by the stability of the formed compound, rather than by the stability of B_4C itself. © *2010 American Institute of Physics*. [doi:10.1063/1.3503521]

I. INTRODUCTION

As a result of the ongoing quest to produce smaller features, the area of application of extreme ultraviolet (EUV, $\lambda = 13.5$ nm) photolithography has expanded in recent years. The viability of EUV technology relies on Mo/Si multilayer reflective optics whose degradation over the desired lifetime of the device is sufficiently low to not impede its operation. Especially under the thermal load induced by the 92 eV EUV radiation, Mo, and Si interdiffuse and form molybdenum silicide compounds. This process alters the period of the multilayer mirror, thus causing a mismatch of the incident radiation and the period thickness. The compound formation furthermore reduces the optical contrast between the layers, therewith decreasing the reflectivity. Especially for many-component optical systems, such as used in EUV lithography, small losses in reflectivity have a major and detrimental impact on the throughput of the equipment.

The degradation of the multilayer optics can be mitigated by the introduction of diffusion barrier layers, such as Si_3N_4, B_4C, and Mo_2C (see, e.g., Refs. 1–3). Literature mostly considers B_4C, describing its effectiveness to increase the stability of the structure without compromising the reflectivity. Recent work[4] concludes that B_4C is chemically reactive with the adjacent Mo and Si layers, without identifying the exact process. Hence, as a logical follow-up, this work focused on the so far largely unknown chemical processes that occur in B_4C-barriered Mo/Si layered structures. This paper also addresses another question arising in this framework, namely, how the chemical behavior of the compound B_4C compares to its constituents B and C in elemental form.

II. EXPERIMENTAL DETAILS

Samples consisting of 10.0 nm Mo/2.0 nm *db*/5.5 nm Si were deposited onto natively oxidized, superpolished Si substrates, where Si is the terminating layer and *db* denotes B, C, or B_4C. Electron beam evaporation was the deposition method of our choice because of the low energy of the particles (~0.1–0.2 eV), thus avoiding particle induced intermixing. Krypton ion beam assistance (beam voltage 80 V, flux 7×10^{13} cm^{-2} s^{-1}, angle of incidence 45°) prevented the build-up of roughness and porosity. The ion beam was switched off during the deposition of the first 1.0 nm of each layer in order to prevent ion induced intermixing at the interfaces. The deposition rate was controlled using a set of four quartz crystal microbalances and fixed at 20 pm/s for Mo, B, C, and B_4C, and 30 pm/s for Si. The base pressure was lower than 1.5×10^{-8} mbar.

The chemical interaction in the samples during annealing was investigated with hard x-ray photoelectron spectroscopy (HAXPES). The higher kinetic energy of photoelectrons in HAXPES with respect to conventional x-ray photoelectron spectroscopy (XPS) increases the mean free path of the photoelectrons. The thus enhanced sampling depth makes HAXPES an especially suitable technique for the investigation of buried interfaces. Moreover, the noninvasive character of HAXPES allows monitoring chemical and compositional changes in real-time.

a)Electronic mail: v.i.t.a.derooij@rijnhuizen.nl.

TABLE I. Overview of the components and associations of the various photoelectron peaks.

Element	Transition	E_{bin} (eV)	Association	Referred to as
Si	2*s*	150.6	Nonoxide, noncarbide	Si_{elem}
		152.4	Carbide, suboxide	$Si_{carb}/Si_{sub\text{-}ox}$
		154.3	Oxide	Si_{oxide}
Mo	$3d_{5/2}$	227.8	Nonoxide	Mo $3d_{5/2}$
	$3d_{3/2}$	230.9	Nonoxide	Mo $3d_{3/2}$
B	1*s*	188.2	Nonoxide	B
C	1*s*	282.6	Carbide	$C_{carbide}$
		284.2	α-C	$C_{amorphous}$

The energy of the incident x-ray radiation used, 2010 eV, results in an attenuation length of 3.7 nm in Si (compare to 2.8 nm for Al K_α radiation),[5] which is sufficient to probe the interface region in the samples. The HAXPES measurements were conducted in real-time during the annealing treatment at the KMC-1 beamline at BESSY II, equipped with the HIKE experimental station. Extensive descriptions of the beamline and the experimental station are given in Refs. 6 and 7, respectively.

The annealing temperature T was in the 400–600 °C range and was adjusted for each sample individually in order to resolve the different processes. Compound formation is judged by changes in binding energy E_{bin} and relative intensity of the photoelectron peaks corresponding to the various elements. Its small cross-section for photoelectric absorption causes a relatively low signal-to-noise ratio for carbon. Consequently, carbon binding energy shifts were below the measurement accuracy, and are, therefore, not reported here. The components of the various photoelectron peaks are listed in Table I, along with the compounds with which they are generally associated. The oxygen signal is not discussed in this paper because, in accordance with the reported stability of SiO_2 in the probed temperature range,[8] no changes in the O 1*s* signal or the oxide-related Si 2*s* peak (at 154.3 eV) were observed. Moreover, no signs of oxidation of Mo, B, or C were found.

The (time-resolved) HAXPES measurements were complemented with depth-resolved information that was obtained by conventional XPS sputter depth profiling. A theta probe instrument and Al K_α radiation ($h\nu$=1486.6 eV) were used for these measurements. Sputter erosion was conducted with 0.5 keV Ar^+ at an angle of 45° with respect to the sample surface. Binding energy shifts and the splitting of peaks in various components were disregarded since compound formation may be caused by the sputter erosion treatment. All samples were analyzed with XPS sputter depth profiling before and after the annealing treatment.

III. RESULTS

The results will be discussed per interlayer material. Starting with the comparatively simple, ternary systems Mo/B/Si and Mo/C/Si, we will conclude with the more complex $Mo/B_4C/Si$ sample. The differences and similarities between the three systems are discussed in Sec. IV.

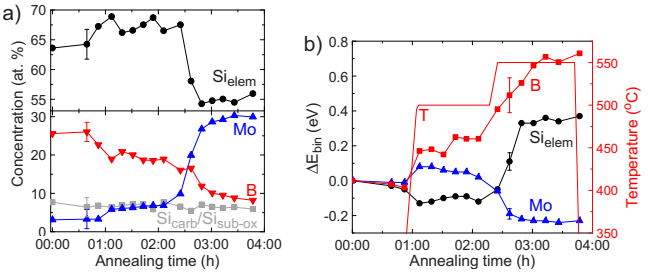

FIG. 1. (Color online) The HAXPES results of the 10.0 nm Mo/2.0 nm B/5.5 nm Si sample as a function of the annealing time. (a) The Si, B, and Mo concentrations, as derived from the relative peak intensities. (b) The binding energy shifts in the B, Si_{elem}, and Mo peaks. The shifts are calculated with respect to the binding energy at t=0. The solid line marked with a T indicates the temperature profile.

A. Mo/B/Si

The HAXPES results of annealing the 10.0 nm Mo/2.0 nm B/5.5 nm Si structure are displayed as a function of the annealing time t in Fig. 1. In view of the absence of C in the structure, the $Si_{carb}/Si_{sub\text{-}ox}$ component is obviously to be fully attributed to silicon suboxide and is only shown for completeness and as a reference for the Mo/C/Si and $Mo/B_4C/Si$ samples. In line with the expected stability of silicon oxide, the $Si_{carb}/Si_{sub\text{-}ox}$ concentration does not change significantly and will, therefore, not be further discussed for this sample. Figure 1 shows that the interaction occurs in two stages: the first stage lasting from approximately t=0:40–2:20 and the second stage from t=2:20–3:00. In the first stage, the B concentration decreases [Fig. 1(a)], while both the B 1*s* E_{bin} and the Mo $3d_{5/2}$ E_{bin} increase [Fig. 1(b)]. Clearly, the B diffuses predominantly away from the surface, toward the Mo layer, and forms molybdenum boride. In addition, the graph shows a simultaneous decrease in the Si_{elem} 2*s* E_{bin}, indicating chemical changes in Si as well. Since the decreasing B concentration indicates that the B diffuses predominantly into the Mo layer, only minor amounts of SiB_x could be formed. Alternatively, the shift in the Si E_{bin} could be caused by decomposition of an SiB_x interfacial layer that had possibly already formed before the start of the annealing treatment.

The second stage sets in when the temperature is increased from 500 to 550 °C at t=2:20. The further decrease in the B concentration indicates diffusion of B further into the Mo layer. Most probably due to a changing stoichiometry of the MoB_x, the B E_{bin} continues to shift positively. Furthermore, the Si concentration drops sharply while the Mo concentration rises. At the same time, the Si_{elem} E_{bin} rises by 0.45 eV while the Mo E_{bin} decreases by 0.25 eV. These changes are a clear signature of molybdenum silicide formation. Literature about similar systems reports that out of the several possible molybdenum silicides, it is (at least predominantly) $MoSi_2$ that is formed.[9,10] The observed binding energy shifts are in accordance with reported, experimentally determined values.[11,12]

The concentration profiles as determined with XPS sputter depth profiling before and after annealing are displayed in Fig. 2. The concentration profile of the sample before annealing [Fig. 2(a)] serves as a reference for the interpretation of

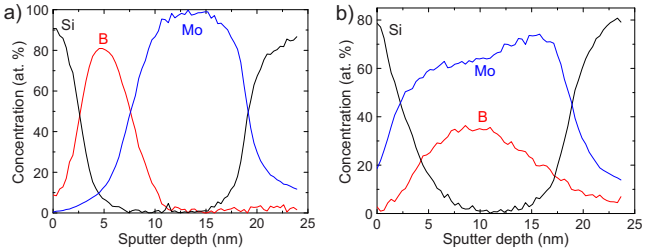

FIG. 2. (Color online) XPS sputter depth profiles of the 10.0 nm Mo/2.0 nm B/5.5 nm Si sample (a) before and (b) after the annealing treatment at the HAXPES facility. Note that the scale of the horizontal axis is indicative only: the erosion rate is calculated from the ion dose assuming a constant sputter yield. The dependency of the sputter yield on the composition of the surface is not taken into account.

the results after the annealing treatment. It shows the deposited structure: Si on B on Mo, on top of the Si substrate. The concentration profiles after annealing [Fig. 2(b)] confirm the previous conclusions: both B and Si have diffused into the Mo layer. Moreover, it is visible that the structure is not homogeneous, but that the $MoSi_x$ layer has formed on top of the MoB_x layer.

The formation of $MoSi_x$ and MoB_x (and not SiB_x) can be explained using the formation enthalpies listed in Table II: it is energetically unfavorable to form SiB_x, because SiB_x has a comparatively small enthalpy of formation ΔH_{form}. Moreover, Si and B are available in smaller quantities than Mo, meaning that SiB_x formation would go at the cost of both $MoSi_x$ and MoB_x formation. Furthermore, the segregation of the MoB_x and $MoSi_x$ in two layers can be attributed to the low solubility of B in $MoSi_x$,[13] and the large interfacial energy associated with a possible eutectic structure. As for the sequence of the two layers: for a $MoSi_x$ on MoB_x structure, the travel distance for Si would be relatively small, because it does not have to travel through the MoB_x layer in order to reach the Mo underneath. In combination with the larger mobility of B with respect to Si,[14] this would cause B rather than Si to diffuse deeper into the Mo layer while $MoSi_x$ forms at the Si/MoB_x interface. This leads to a $MoSi_x$ on MoB_x structure, which is fully in line with the observations.

B. Mo/C/Si

Figure 3 displays the HAXPES results of annealing the sample with 10.0 nm Mo/2.0 nm C/5.5 nm Si. The graphs

TABLE II. Literature values for the formation enthalpies ΔH_{form} of relevant compounds.

	ΔH_{form} at 298 K (kJ/mole atoms)	Reference
B_4C	−11	15
Mo_2C	−16	16
SiB_3	−23	17
Mo_3Si	−29	18
SiC	−36	18
Mo_5Si_3	−39	18
$MoSi_2$	−44	18
Mo_2B_5	−54	16
MoB_2	−57	16
MoB	−62	16

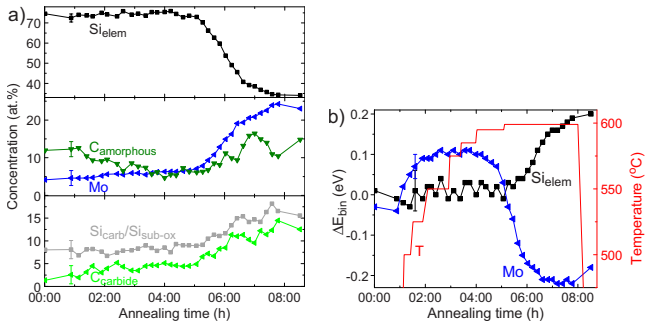

FIG. 3. (Color online) The HAXPES results of the 10.0 nm Mo/2.0 nm C/5.5 nm Si sample as a function of the annealing time. (a) The Si, C, and Mo concentrations, as derived from the relative peak intensities. (b) The binding energy shifts in the Si_{elem} and Mo peaks. The shifts are calculated with respect to the same binding energies as in Fig. 1(b). The solid line marked with a *T* indicates the temperature profile.

show that the interaction in this sample also occurs in two stages: the first stage lasts from approximately $t=0:50-5:00$ and the second stage from $t=5:00-7:00$. In the first stage, the concentration of $C_{carbide}$ rises at the cost of $C_{amorphous}$ [Fig. 3(a)], while the Mo E_{bin} increases [Fig. 3(b)]. This indicates that C diffuses away from the surface, i.e., toward the Mo layer, and forms molybdenum carbide. The positive shift in the Mo E_{bin} is in agreement with the findings of Brainard and Wheeler.[11] There are no indications for chemical processes involving Si, since neither its concentration (Si_{elem} nor Si_{carb}/Si_{sub-ox}), nor its binding energy changes significantly. Moreover, the Si_{carb}/Si_{sub-ox} concentration is the same as in the sample with B interlayer, indicating that it can be fully attributed to silicon suboxide, and does not point toward the presence or formation of silicon carbide.

The second stage sets in when the temperature is increased to 600 °C. Together with the E_{bin} shifts in Mo and Si_{elem}, the rise of the Mo concentration and the decrease in the Si_{elem} concentration indicate $MoSi_x$ formation. Rather surprisingly, the concentrations of $Si_{carbide}$ and $C_{carbide}$ increase at the same time, indicating that SiC_x forms, or that an already formed SiC_x comes closer to the surface, because elemental Si diffuses deeper in the structure.

The results of the sputter depth profiling analysis of the sample before and after the annealing treatment are shown in Fig. 4. The concentration profile of the sample before annealing serves as a reference for the interpretation of the results after the annealing treatment. Before annealing [Fig. 4(a)],

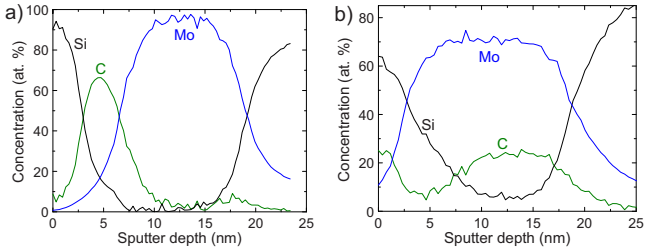

FIG. 4. (Color online) XPS sputter depth profiles of the 10.0 nm Mo/2.0 nm C/5.5 nm Si sample (a) before and (b) after the annealing treatment at the HAXPES facility. Note that the scale of the horizontal axis is indicative only: the erosion rate is calculated from the ion dose assuming a constant sputter yield. The dependency of the sputter yield on the composition of the surface is not taken into account.

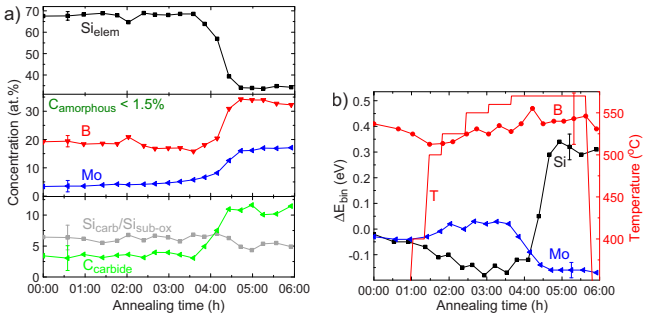

FIG. 5. (Color online) The HAXPES results of the 10.0 nm Mo/2.0 nm B_4C/5.5 nm Si sample as a function of the annealing time. (a) The Si, B, C, and Mo concentrations, as derived from the relative peak intensities. (b) The binding energy shifts in the B, Si_{elem}, and Mo peaks. The shifts are calculated with respect to the same binding energies as in Fig. 1(b). The solid line marked with a *T* indicates the temperature profile.

the graph shows the deposited structure: Si on C on Mo, on top of the Si substrate. After annealing [Fig. 4(b)], a SiC_x layer is visible on top of $MoSi_2$ on top of MoC_x. Combining this with the HAXPES results, we can conclude that, besides MoC_x, SiC_x formed at the interface, either during the deposition or in the course of the annealing. Apparently, this SiC_x is stable and, in stage 2, the elemental Si diffuses *through* this compound to form $MoSi_2$, leaving SiC_x near the surface of the sample.

The formation of SiC and $MoSi_2$ can be explained using the thermodynamic data listed in Table II: for the available amounts of material, $MoSi_2$ and SiC formation are favorable over Mo_2C formation. However, we observed that the majority of the C bonds to Mo rather than to Si. We can explain this by assuming that SiC is not permeable to C once it reaches a certain thickness. Therefore, only part of the C is able to form SiC. The remainder of the C would then react with Mo, the only other element available. In stage 2, Si diffuses through SiC, so that $MoSi_2$ can be formed and Mo_2C segregates toward the wafer.

Note that the observed stability of SiC_x in contact with $MoSi_x$ is in accordance with the results of Amrani *et al.*[19] and Boettinger *et al.*,[20] who report that SiC in contact with $MoSi_2$ is stable at 1200 °C and 1600 °C, respectively.

Figure 4(b) further shows that the $MoSi_x$ and MoC_x have segregated in separate layers. This segregation has also been observed in Ref. 21 and can be attributed to the same causes as the segregation of MoB_x in the previously discussed sample: a large interfacial energy associated with a possible eutectic structure, and, presumably, a low solubility of C in $MoSi_x$/Si in MoC_x. Finding $MoSi_x$ on top of MoC_x and not vice versa is presumably caused by the fact that Si needs to travel a smaller distance. In combination with the higher mobility of C compared to Si, this causes C rather than Si to diffuse deeper into the Mo layer when $MoSi_x$ forms at the Si/MoC_x interface.

C. Mo/B_4C/Si

Figure 5 displays the HAXPES results of annealing the sample with 10.0 nm Mo/2.0 nm B_4C/5.5 nm Si. The graphs show that also in this structure the interaction occurs in two stages: the first stage lasts from approximately *t* =0:30–3:40 and the second stage from *t*=3:40–5:00. Note that because B is in a compound instead of in its elemental form, the B E_{bin} is high compared to the Mo/B/Si sample at *t*=0.

The changes in the first stage are small. Nevertheless, the gradual decrease in the B concentration and the gradual increase in the Mo concentration [Fig. 5(a)] are significant and suggest that B diffuses away from the surface, into the Mo layer, thus forming MoB_x. This is supported by the positive shift in the Mo E_{bin} [Fig. 5(b)], although it may also be (partially) caused by MoC_x formation. The B E_{bin} does not change significantly, while the results from the Si/B/Mo sample indicate that MoB_x formation should reduce the shift to 0.2 eV. This is due to the fact that the majority of the B signal does not stem from the B that diffused into the Mo but from B that remained at the interface. We will show below that this B is still bond to C, which explains why the B E_{bin} still corresponds to that of B in B_4C. Because no E_{bin} reference values are available, we cannot, at this point, conclude whether it concerns a pure B_xC compound or rather a SiB_xC_y compound.

Finally, the decrease in the Si E_{bin} in stage 1 is inconclusive as it suggests either SiB_x formation in a small quantity or decomposition (see Sec. III A). Neither the $Si_{carb}/Si_{sub\text{-}ox}$ nor the $C_{carbide}$ concentration profile reveals signs of SiC_x formation. We remark that it is very well possible that ternary compounds like MoB_xC_y and SiB_xC_y formed besides these binary compounds. However, they cannot be identified through their binding energy shifts because no reference values are available.

The second stage sets in at *t*=3:40, when the temperature is increased to 570 °C. The E_{bin} shifts in Mo and Si_{elem}, the rise of the Mo concentration and the decrease in the Si_{elem} concentration together indicate $MoSi_x$ formation. Moreover, the concentrations of both $C_{carbide}$ and B increase at the same time, indicating that boron carbide comes closer to the surface. Furthermore, it is apparent from the reduction in the B:C ratio by a factor of 2 between *t*=3:40 and 4:30 that the boron carbide has become poorer in B. However, the B E_{bin} does not shift significantly, which suggests that the probed B is not present in MoB_x or $MoSi_xB_y$, but in SiB_xC_y or perhaps still in a remaining part of boron carbide. This indicates that Si diffuses through the remainder of the boron carbide or SiB_xC_y layer at the interface to form $MoSi_x$, thus enhancing the B and C signal intensities by bringing the boron carbide or SiB_xC_y layer closer to the surface.

The results of the sputter depth profiling analysis of the sample before and after the annealing treatment are shown in Fig. 6. Before annealing [Fig. 6(a)], the graph shows the deposited structure: Si on B_4C on Mo, on top of the Si substrate. After annealing [Fig. 6(b)], a SiB_xC_y layer is visible on top of $MoSi_x$ (or possibly $MoSi_xB_y$) on MoB_xC_y. The latter becomes poorer in B and richer in C toward the substrate and may even consist of separate layers of MoB_x and MoC_x.

Since the HAXPES results in Fig. 5 indicate a B_xC or SiB_xC_y layer close to the surface after annealing, it is plausible that the B has split into two parts. One part remained B_xC or formed SiB_xC_y, while the other part diffused into Mo

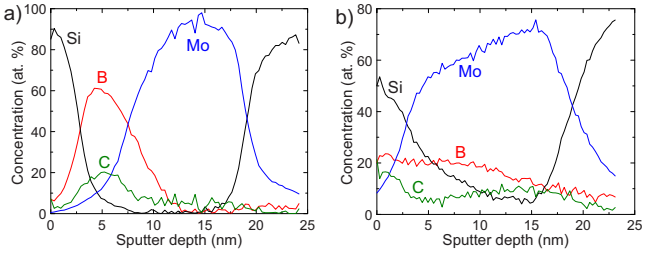

FIG. 6. (Color online) XPS sputter depth profiles of the 10.0 nm Mo/2.0 nm B_4C/5.5 nm Si sample (a) before and (b) after the annealing treatment at the HAXPES facility. Note that the scale of the horizontal axis is indicative only: the erosion rate is calculated from the ion dose assuming a constant sputter yield. The dependency of the sputter yield on the composition of the surface is not taken into account.

during the first stage and segregated toward the substrate in the second stage. In order to verify the chemical state of B after annealing at different depths, we split the B peak in the XPS depth profile into two components, each with fixed E_{bin}: B_+ at 188.7 eV and B_- at 187.7 eV. The result is shown in Fig. 7. Note that the extent to which the results are affected by the sputter-induced intermixing artifacts are unknown. Nevertheless, Fig. 7 clearly supports the hypothesis of the split B distribution suggested by the HAXPES results: a B_+ distribution is found close to the surface, and can be associated with B_xC or SiB_xC_y. The B_- distribution on the other hand is located deeper in the sample, below the $MoSi_x$ layer, and is hence associated with MoB_x.

Combining the depth profiling results with the HAXPES results, we can conclude that, besides MoB_xC_y (or MoB_x plus MoC_x), B_xC and/or SiB_xC_y formed at the interface. The latter compound is stable, and in the second stage the elemental Si diffuses through this compound to form $MoSi_2$, leaving B_xC and/or SiB_xC_y near the surface of the sample. Furthermore, the mobility of B and C is larger than that of Si, which causes segregation of MoB_xC_y (or MoB_x plus MoC_x) when $MoSi_x$ forms at the interface.

IV. DISCUSSION

After the description and identification of the processes that occur in the investigated samples, this section focuses on the comparison between the interaction of B, C, and B_4C interlayers with Mo and Si.

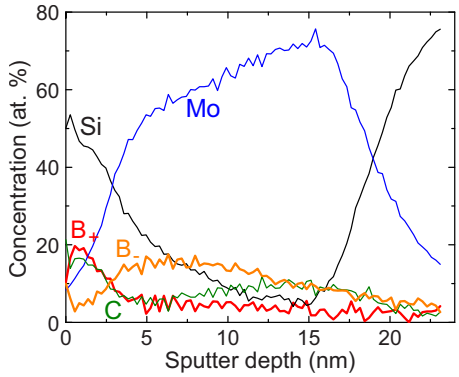

FIG. 7. (Color online) XPS sputter depth profiles of the 10.0 nm Mo/2.0 nm B_4C/5.5 nm Si sample after the annealing treatment at the HAXPES facility. This figure is identical to Fig. 6(b), except that the B peak is now split into two components, where B_+ can be associated with B_xC/SiB_xC_y, and B_- with MoB_x/MoB_xC_y.

In all three systems, the first interaction to occur is that of the interlayer with Mo and, to a lesser extent, with Si. Another process the systems have in common is the formation of $MoSi_x$ with x close to 2, and the segregation of MoB_x/MoC_x that it induces. A major difference between the samples with elemental C and B barriers is that only in the former case a stable compound (SiC_x) is formed, through which Si diffuses to form $MoSi_x$ in the second stage. No indications were observed that C behaves differently in the presence of B: both in the C and in the B_4C sample, C partially diffuses into the Mo and partially into Si, where it forms a stable compound. The behavior of B, on the contrary, is obviously affected by the presence of C: in the Mo/B_4C/Si system, only part of the B (B_- in Fig. 7) behaves similar to B in the Mo/B/Si system and forms MoB_x. The other part though (B_+ in Fig. 7) remains bonded to C and is encountered close to the surface after the annealing treatment. It answers the question posed in the introductory section, whether the interaction of B_4C is fundamentally different from that of B or C with Mo and Si: the compounds formed with involvement of C are significantly more stable. This difference is likely to make the barrier functionality of B interlayers inferior to that of C or B_4C interlayers. Furthermore, we suggest here that the diffusion barrier function of B_4C interlayers as reported in literature can be caused by the stability of the formed boron-poor B_xC/SiB_xC_y layer, rather than the stability of the B_4C layer itself. In fact, this layer most probably consists of SiB_xC_y rather than B_xC, as it is unlikely that off-stoichiometric B_xC is more stable than stoichiometric B_4C.

We performed simulations to investigate whether the SiB_xC_y compound may have formed due to the 80 eV krypton ion bombardment during the deposition of the Si layer onto the C/B_4C layer. The penetration depth of these ions was evaluated via molecular dynamics simulations of the effect of bombarding amorphous silicon with 400 Kr atoms. The Kr atoms had a kinetic energy of 80 eV and the sample consisted of a 8.1×8.1 nm^2 Si(001) crystal with an amorphous top layer of 3.0 nm thick. See Ref. 22 for extensive details about the sample structure and the Si and Si–Kr potentials. The temperature was 27 °C and the interval between two impacts was 7.1 ps. As during the real deposition, the polar angle of incidence was 45°, with random azimuth. The main result of these simulations is that the penetration depth of the ions was 0.73 nm with a root-mean-square variation in 0.3 nm. This makes the ion bombardment unlikely as a cause of the SiB_xC_y compound formation, since the ion bombardment only started at a Si layer thickness of 1.0 nm. Hence, we can conclude that the SiB_xC_y formed spontaneously, either during deposition or during the first stage of the annealing treatment.

We furthermore like to remark that the results of experiments with a reverse layer sequence (i.e., Si/interlayer/Mo instead of Mo/interlayer/Si) are consistent with the above mentioned conclusions: depth profiling of annealed Si/C/Mo and Si/B_4C/Mo structures showed split C/B profiles, while B was only observed in the Mo layer after annealing of a Si/B/Mo sample.

As a final remark, it was observed for all three systems

that the transition to the second stage was triggered by the raise in temperature. However, since time and temperature are generally interchangeable, it is most likely that if the temperature had not been raised, the same chemical changes would have occurred, albeit at a substantially longer timescale.

V. CONCLUSIONS

The chemical processes occurring in Mo/B/Si, Mo/C/Si, and $Mo/B_4C/Si$ layered structures upon annealing up to 600 °C have been identified using XPS depth profiling and *in situ* HAXPES. The first process to take place is B (respectively, C) diffusing into Mo to form predominantly MoB_x (respectively, MoC_x and MoB_xC_y). In addition, possibly small amounts of SiB_x (respectively, SiC_x and SiB_xC_y) are formed. Subsequently, upon raising the annealing temperature, Si is able to diffuse toward Mo. The already formed MoB_x (respectively, MoC_x and MoB_xC_y) decomposes in favor of $MoSi_x$ formation. The released B (respectively, C) diffuses further forming MoB_x (respectively, MoC_x and MoB_xC_y) deeper into the Mo layer. Only when the barrier layer contains C, the barrier layer material forms a compound (SiC_x respectively, SiB_xC_y) that is stable up to the maximum probed temperature and annealing time. We suggest that in view of the stability of the SiB_xC_y layer, the diffusion barrier function of B_4C interlayers as reported in literature can be caused by the stability of the formed SiB_xC_y layer, rather than the stability of the B_4C layer itself. In the second stage, Si diffuses through the compound layer to form $MoSi_x$. In this sense, the interaction of B_4C with Mo and Si is similar to C rather than to B.

ACKNOWLEDGMENTS

This work is part of the FOM Industrial Partnership Programme I10 ('XMO') which is carried out under contract with Carl Zeiss SMT AG, Oberkochen, and the "Stichting voor Fundamenteel Onderzoek der Materie (FOM)," the latter being financially supported by the "Nederlandse Organisatie voor Wetenschappelijk Onderzoek (NWO)." The HAXPES research leading to these results have received funding from the European Community's Seventh Framework Programme (FP7/2007-2013) under Grant agreement No. 226716.

[1] I. Nedelcu, R. W. E. van de Kruijs, A. E. Yakshin, and F. Bijkerk, J. Appl. Phys. **103**, 083549 (2008).
[2] S. Bajt, J. B. Alameda, T. W. Barbee, W. M. Clift, J. A. Folta, B. Kaufmann, and E. A. Spiller, Opt. Eng. **41**, 1797 (2002).
[3] T. Feigl, S. Yulin, N. Kaiser, and R. Thielsch, *Emerging Lithographic Technologies IV* (SPIE, Santa Clara, 2000), Vol. 3997, p. 420.
[4] V. I. T. A. de Rooij-Lohmann, A. E. Yakshin, R. W. E. van de Kruijs, E. Zoethout, A. W. Kleyn, E. G. Keim, M. Gorgoi, F. Schäfers, H. H. Brongersma, and F. Bijkerk, J. Appl. Phys. **108**, 014314 (2010).
[5] P. J. Cumpson and M. P. Seah, Surf. Interface Anal. **25**, 430 (1997).
[6] F. Schaefers, M. Mertin, and M. Gorgoi, Rev. Sci. Instrum. **78**, 123102 (2007).
[7] M. Gorgoi, S. Svensson, F. Schäfers, G. Öhrwall, M. Mertin, P. Bressler, O. Karis, H. Siegbahn, A. Sandell, H. Rensmo, W. Doherty, C. Jung, W. Braun, and W. Eberhardt, Nucl. Instrum. Methods Phys. Res. A **601**, 48 (2009).
[8] V. I. T. A. de Rooij-Lohmann, A. W. Kleyn, F. Bijkerk, H. H. Brongersma, and A. E. Yakshin, Appl. Phys. Lett. **94**, 063107 (2009).
[9] J. Y. Cheng, H. C. Cheng, and L. J. Chen, J. Appl. Phys. **61**, 2218 (1987).
[10] A. Guivarc'h, P. Auvray, L. Berthou, M. Le Cun, J. P. Boulet, P. Henoc, G. Pelous, and A. Martinez, J. Appl. Phys. **49**, 233 (1978).
[11] W. A. Brainard and D. R. Wheeler, J. Vac. Sci. Technol. **15**, 1800 (1978).
[12] K. Hirose, I. Ohdomari, and M. Uda, Phys. Rev. B **37**, 6929 (1988).
[13] H. Nowotny, E. Dimakopoulou, and H. Kudielka, Monatsch. Chem. **88**, 180 (1957).
[14] The larger mobility of B with respect to Si is apparent from the fact that B diffuses at a lower T than Si.
[15] J. E. Saal, S. Shang, and Z.-K. Liu, Appl. Phys. Lett. **91**, 231915 (2007).
[16] F. R. de Boer, R. Boom, W. C. M. Mattens, A. R. Miedema, and A. K. Niessen, *Cohesion in Metals: Transition Metal Alloys* (North-Holland, Amsterdam, 1988).
[17] H. M. Chen, H. Y. Qi, F. Zheng, L. B. Liu, and Z. P. Jin, J. Alloys Compd. **481**, 182 (2009).
[18] A. Costa e Silva and M. J. Kaufman, Metall. Mater. Trans. A **25**, 5 (1994).
[19] H. Amrani, R. Hillel, F. Sibieude, R. Berjoan, and R. Verges, J. Mater. Sci. Lett. **13**, 1472 (1994).
[20] W. J. Boettinger, J. H. Perepezko, and P. S. Frankwicz, Mater. Sci. Eng., A **155**, 33 (1992).
[21] P. Steinmetz, B. Roques, and R. Pichoir, J. Less-Common Met. **48**, 225 (1976).
[22] M. Timonova, B.-J. Lee, and B. J. Thijsse, Nucl. Instrum. Methods Phys. Res. B **255**, 195 (2007).